optica

Robustness of entanglement as an indicator of topological phases in quantum walks: supplementary material

QIN-QIN WANG[1,2], XIAO-YE XU[1,2*], WEI-WEI PAN[1,2], SI-JING TAO[1,2], ZHE CHEN[1,2], YONG-TAO ZHAN[1,2], KAI SUN[1,2], JIN-SHI XU[1,2], GENG CHEN[1,2], YONG-JIAN HAN[1,2†], CHUAN-FENG LI[1,2‡], AND GUANG-CAN GUO[1,2]

[1]CAS Key Laboratory of Quantum Information, University of Science and Technology of China, Hefei 230026, People's Republic of China
[2]CAS Center For Excellence in Quantum Information and Quantum Physics, University of Science and Technology of China, Hefei 230026, People's Republic of China

[*]Corresponding author: xuxiaoye@ustc.edu.cn
[†]Corresponding author: smhan@ustc.edu.cn
[‡]Corresponding author: cfli@ustc.edu.cn

Published 14 January 2020

This document provides supplementary information to "Robustness of entanglement as an indicator of topological phases in quantum walks, https://doi.org/10.1364/OPTICA.375388." We provide the detailed physical descriptions of the connection between the topological robustness and the resulting robustness of entangle-ment, and show our work can be extended to some other Floquet systems.

1. THE RELATION BETWEEN THE WINDING NUMBERS AND THE ROBUSTNESS OF ASYMPTOTIC ENTANGLEMENT IN QUANTUM WALKS.

For simplification, we firstly begin with considering a local initial state $|x=0\rangle \otimes |\downarrow_y\rangle$. The initial density matrix of the spin (coin) in the momentum space takes the form $\rho_i(k) = \frac{1}{2}[\mathbb{1} + \boldsymbol{d}_i(k)\cdot\hat{\sigma}]$, where $\mathbb{1}$ is the identity matrix, $\boldsymbol{d}_i(k) = (0,1,0)$ is the Bloch vector for momentum k and $\hat{\sigma}$ is the Pauli vector. At any given time t, the density matrix of the coin for momentum k can be formally written as: $\rho(k,t) = \frac{1}{2}[\mathbb{1} + \boldsymbol{d}(k,t)\cdot\hat{\sigma}]$, where the Bloch vector $\boldsymbol{d}(k,t)$ is given by [1]:

$$\begin{aligned}\boldsymbol{d}(k,t) =& \boldsymbol{d}_i(k)\cos[2E(k)t] + 2\boldsymbol{n}(k)[\boldsymbol{d}_i(k)\cdot\boldsymbol{n}(k)]\sin^2[E(k)t] \\ &+ \boldsymbol{n}(k)\times\boldsymbol{d}_i(k)\sin[2E(k)t].\end{aligned} \tag{S1}$$

$\boldsymbol{d}_i(k)$ is the initial Bloch vector of the coin ($(0,1,0)$ in our current case), $\boldsymbol{n}(k)$ is the eigenvector of the effective Hamiltonian $H_{\text{eff}}(k)$ in the split-step quantum walks. For the quantum walks introduced in the main text, it can be written as [2, 3]:

$$\begin{aligned} n_x &= \frac{\sin(\theta_1/2)\cos(\theta_2/2)\sin k}{\sin[E(k)]} \\ n_y &= \frac{\sin(\theta_1/2)\cos(\theta_2/2)\cos k + \cos(\theta_1/2)\sin(\theta_2/2)}{\sin[E(k)]} \\ n_z &= \frac{-\cos(\theta_1/2)\cos(\theta_2/2)\sin k}{\sin[E(k)]} \end{aligned} \tag{S2}$$

where $E(k)$ represents the quasi-energy and defined as:

$$\cos[E(k)] = \cos(\theta_1/2)\cos(\theta_2/2)\cos k - \sin(\theta_1/2)\sin(\theta_2/2). \tag{S3}$$

Since we only consider the asymptotic behavior of the walk, we get the reduced density matrix of the coin in the long-time limit as:

$$\begin{aligned}\overline{\rho}_C &= \frac{1}{2}[\mathbb{1} + \int_{-\pi}^{\pi}\frac{dk}{2\pi}(\boldsymbol{d}_i(k)\cdot\boldsymbol{n}(k))\boldsymbol{n}(k)\cdot\hat{\sigma})] \\ &= \frac{1}{2}[\mathbb{1} + \int_{-\pi}^{\pi}\frac{dk}{2\pi}(n_y(k)\boldsymbol{n}(k))\cdot\hat{\sigma})].\end{aligned} \tag{S4}$$

It has been shown in Ref. [4] that the entanglement of the whole quantum state $\overline{\rho}$, quantified by the von Neumann entropy

$S_E[\bar{\rho}]$, can be expressed as a function of the polarization purity (PP), which is defined as the length of the Bloch vector of $\bar{\rho}_C$ (denotes as $\mathcal{P}[\bar{\rho}_C]$). That is, we can rewrite the von Neumann entropy in terms of $\mathcal{P}[\bar{\rho}_C]$ as:

$$S_E[\bar{\rho}] = -\frac{1}{2}\log_2(\frac{1-\mathcal{P}[\bar{\rho}_C]^2}{4}) - \frac{1}{2}\mathcal{P}[\bar{\rho}_C]\log_2(\frac{1+\mathcal{P}[\bar{\rho}_C]}{1-\mathcal{P}[\bar{\rho}_C]}). \tag{S5}$$

Therefore, the robustness of entanglement is equivalent to the robustness of the corresponding PP.

From Eq. S4 and its definition, PP can be directly given in terms of the spinor eigenvector as:

$$\mathcal{P}[\bar{\rho}_C] = |\int_{-\pi}^{\pi}\frac{dk}{2\pi}(n_y(k)\boldsymbol{n}(k))| = \int_{-\pi}^{\pi}\frac{dk}{2\pi}|n_y(k)|^2$$
$$= \int_{-\pi}^{\pi}\frac{dk}{2\pi}\frac{[\cos(\theta_1/2)\sin(\theta_2/2)+\sin(\theta_1/2)\cos(\theta_2/2)\cos k]^2}{1-[\cos(\theta_1/2)\cos(\theta_2/2)\cos k-\sin(\theta_1/2)\sin(\theta_2/2)]^2}. \tag{S6}$$

By introducing $z = e^{ik}$ in the complex plane, we can apply the residue theorem to calculate the integral, and PP is then given by $\mathcal{P}[\bar{\rho}_C] = \oint_{|z|=1} dz f(z)/(2\pi\mathrm{i})$, where

$$f(z) = \frac{4z[\cos(\theta_1/2)\sin(\theta_2/2)+\sin(\theta_1/2)\cos(\theta_2/2)(\frac{z+\frac{1}{z}}{2})]^2}{4z^2-[(1+z^2)\cos(\theta_1/2)\cos(\theta_2/2)-2z\sin(\theta_1/2)\sin(\theta_2/2)]^2}. \tag{S7}$$

The complex function above has five poles,

$$\begin{aligned}
z_0 &= 0,\\
z_1 &= \frac{\sin(\theta_1/2)\sin(\theta_2/2)-1+[\sin(\theta_1/2)-\sin(\theta_2/2)]}{\cos(\theta_1/2)\cos(\theta_2/2)},\\
z_2 &= \frac{\sin(\theta_1/2)\sin(\theta_2/2)-1-[\sin(\theta_1/2)-\sin(\theta_2/2)]}{\cos(\theta_1/2)\cos(\theta_2/2)},\\
z_3 &= \frac{\sin(\theta_1/2)\sin(\theta_2/2)+1-[\sin(\theta_1/2)+\sin(\theta_2/2)]}{\cos(\theta_1/2)\cos(\theta_2/2)},\\
z_4 &= \frac{\sin(\theta_1/2)\sin(\theta_2/2)+1+[\sin(\theta_1/2)+\sin(\theta_2/2)]}{\cos(\theta_1/2)\cos(\theta_2/2)}.
\end{aligned} \tag{S8}$$

And the corresponding residues of $f(z)$ at the poles are given by:

$$\begin{aligned}
\mathrm{Res}[z_0] &= -\tan^2(\theta_1/2),\\
\mathrm{Res}[z_1] &= \frac{\sin(\theta_1/2)-\sin(\theta_2/2)}{2\cos^2(\theta_1/2)},\\
\mathrm{Res}[z_2] &= \frac{-\sin(\theta_1/2)+\sin(\theta_2/2)}{2\cos^2(\theta_1/2)},\\
\mathrm{Res}[z_3] &= \frac{\sin(\theta_1/2)+\sin(\theta_2/2)}{2\cos^2(\theta_1/2)},\\
\mathrm{Res}[z_4] &= \frac{-\sin(\theta_1/2)-\sin(\theta_2/2)}{2\cos^2(\theta_1/2)}.
\end{aligned} \tag{S9}$$

Note that only the poles inside the unit circle $|z| = 1$ contribute to the value of PP, from which we can establish the relation between PP and the winding number of quantum walks.

In quantum walks, the trajectory of eigenvector $\boldsymbol{n}(k)$ winds around the vector $\mathbf{A}(\theta_1) = (\cos(\theta_1/2), 0, \sin(\theta_1/2))$ on the Bloch sphere when k goes from $-\pi$ to π. Actually, the vector $\mathbf{A}(\theta_1)$ defines the chiral symmetry supported by the quantum walks. Therefore, the trajectory of eigenvector $\boldsymbol{n}(k)$ is fixed on a plane containing the y-axis and perpendicular to $\mathbf{A}(\theta_1)$. When the trajectory of $\boldsymbol{n}(k)$ forms a closed circle, its winding number $\mathcal{W} = 1$, while $\mathcal{W} = 0$ when trajectory is an arc. With the expression of $\boldsymbol{n}(k)$, it is clear that $\boldsymbol{n}(k)$ and $\boldsymbol{n}(-k)$ are symmetry along the y-axis, i.e. $n_y(k) = n_y(-k)$. In addition, $n_x(0) = n_x(\pi) = 0$ and $n_z(0) = n_z(\pi) = 0$, thus $\boldsymbol{n}(0)$ and $\boldsymbol{n}(\pi)$ are on the y-axis and they can only parallel or anti-parallel.

Therefore, the relation of $\boldsymbol{n}(0)$ and $\boldsymbol{n}(\pi)$ is directly corresponding to the winding number of the trajectory of $\boldsymbol{n}(k)$: if they are parallel, the $\boldsymbol{n}(\pi)$ is back to the initial $\boldsymbol{n}(0)$ and the trajectory of $\boldsymbol{n}(k)$ can not form a closed circle ($\mathcal{W} = 0$); on the other hand, if they are anti-parallel, $\boldsymbol{n}(\pi)$ and $\boldsymbol{n}(0)$ are two opposite vectors and the trajectory of $\boldsymbol{n}(k)$ forms a closed circle ($\mathcal{W} = 1$).

As a result, the winding number (i.e. the parallel or anti-parallel relation between $\boldsymbol{n}(0)$ and $\boldsymbol{n}(\pi)$) can be determined by the sign of

$$\boldsymbol{n}(0)\cdot\boldsymbol{n}(\pi) = \frac{\sin^2(\theta_2/2)\cos^2(\theta_1/2)-\cos^2(\theta_2/2)\sin^2(\theta_1/2)}{\sqrt{1-(\cos[(\theta_2-\theta_1)/2)^2}\sqrt{1-(\cos[(\theta_2+\theta_1)/2)^2}}. \tag{S10}$$

If $\boldsymbol{n}(0)\cdot\boldsymbol{n}(\pi) < 0$, i.e $|\tan(\theta_2/2)/\tan(\theta_1/2)| < 1$, $\boldsymbol{n}(0)$ and $\boldsymbol{n}(\pi)$ are anti-parallel; while $\boldsymbol{n}(0)\cdot\boldsymbol{n}(\pi) > 0$, that is, $|\tan(\theta_2/2)/\tan(\theta_1/2)| > 1$, $\boldsymbol{n}(0)$ and $\boldsymbol{n}(\pi)$ are parallel. Thus, if the winding number $\mathcal{W} = 1$, $|\tan(\theta_2/2)/\tan(\theta_1/2)| < 1$; if the winding number $\mathcal{W} = 0$, $|\tan(\theta_2/2)/\tan(\theta_1/2)| > 1$ and vice versa.

With the previous analysis, when the winding number $\mathcal{W} = 1$, only the poles $\{z_0, z_1, z_3\}$ (when $\theta_1 \geq 0$), or $\{z_0, z_2, z_4\}$ (when $\theta_1 < 0$) are inside the unit circle $|z| = 1$ (note that the poles z_1 and z_3, z_2 and z_4 are paired to cancel the effect of θ_2); meanwhile, when the winding number $\mathcal{W} = 0$, only poles $\{z_0, z_1, z_4\}$ (when $\theta_2 < 0$) or $\{z_0, z_2, z_3\}$ (when $\theta_2 \geq 0$) are inside the unit circle $|z| = 1$ (see Fig. 1). Therefore, via calculating the residues, we can get the analytical expressions for $\mathcal{P}[\bar{\rho}_C]$:

$$\begin{aligned}
\mathcal{P}[\bar{\rho}_C] &= \begin{cases} \mathrm{Res}[z_0]+\mathrm{Res}[z_{1(2)}]+\mathrm{Res}[z_{3(4)}], \\ \mathrm{Res}[z_0]+\mathrm{Res}[z_{1(2)}]+\mathrm{Res}[z_{4(3)}], \end{cases}\\
&= \begin{cases} \frac{-\sin^2(\theta_1/2)+\sin(|\theta_1|/2)}{\cos^2(\theta_1/2)} & ,|\tan(\frac{\theta_2}{2})/\tan(\frac{\theta_1}{2})| < 1. \\ \frac{-\sin^2(\theta_1/2)+\sin(|\theta_2|/2)}{\cos^2(\theta_1/2)} & ,|\tan(\frac{\theta_2}{2})/\tan(\frac{\theta_1}{2})| > 1. \end{cases}
\end{aligned} \tag{S11}$$

From these expressions, it is clear that, when the winding number $\mathcal{W} = 1$, the PP and entanglement are only dependent on the parameter θ_1 and robust against the perturbation of parameter θ_2. However, when the winding number $\mathcal{W} = 0$, the PP and entanglement are dependent on both parameters θ_1 and θ_2.

In addition, the robustness of PP can also be closely related to the stability of the energy range covered by the band ($|E(\pi) - E(0)|$) through group velocity [5]. To establish their connection, we use the relations, $n_z(k) = -n_x(k)/\tan(\theta_1/2) = -dE(k)/dk$, where $dE(k)/dk$ is the associated group velocity

$v_g(k)$, and $n_y^2(k) = 1 - n_x^2(k) - n_z^2(k)$ to rewrite PP as:

$$\begin{aligned}\mathcal{P}[\overline{\rho}_C] &= 1 - [1+\tan^2(\theta_1/2)]\int_{-\pi}^{\pi}\frac{dk}{2\pi}|v_g(k)|^2 \\ &= 1 - [1+\tan^2(\theta_1/2)]\left\{1-\sin[\frac{\pi-|E(\pi)-E(0)|}{2}]\right\} \\ &= \begin{cases} 1-[1+\tan^2(\theta_1/2)] & \\ \times\left\{1-\sin[\frac{\pi-\left|\pi-|\theta_1|\right|}{2}]\right\} & |\tan(\frac{\theta_2}{2})/\tan(\frac{\theta_1}{2})|<1, \\ 1-[1+\tan^2(\theta_1/2)] & \\ \times\left\{1-\sin[\frac{\pi-\left|\pi-|\theta_2|\right|}{2}]\right\} & |\tan(\frac{\theta_2}{2})/\tan(\frac{\theta_1}{2})|>1. \end{cases}\end{aligned} \tag{S12}$$

In Fig. 2, we collect the different behaviors of the winding of $\boldsymbol{n}(k)$, the quasi-energy $E(k)$ and $n_y(k)$ as a function of the quasi-momentum k in different topological phases. To make it clear, we fix the parameter $\theta_1 = \pi/2$ and focus on the parameter θ_2. Note that fixing the value of θ_1 means fixing the symmetrical axis $\boldsymbol{A}(\theta_1)$ [2, 3] which determines the chiral symmetry.

It can be clearly seen that, in the trivial topological phase, the winding of $\boldsymbol{n}(k)$ forms an *arc* on the surface of Bloch sphere with a θ_2-dependent length. The arc length can change from long to short (even degenerates to zero, i.e., a single point) when varying θ_2, and correspondingly, the energy range covered by the band ($|E(\pi) - E(0)|$) increases or decreases within the two regions $\{-\pi, -\pi/2\}$ and $\{\pi/2, \pi\}$. At the same time, $n_y(k)$ occupies a limited area along the y-axis. On the contrary, in the non-trivial topological phase, the vector $\boldsymbol{n}(k)$ winds around the origin forming a closed circle. The energy band only shifts with minor deformations when changing θ_2 and always covers a stable range of energy. And the associated y-component $n_y(k)$ always fill up the y axis.

The method outlined above can be easily applied to scenarios with any localized initial state (just by replacing $n_y(k)$ with $\boldsymbol{d}_i(k)\cdot\boldsymbol{n}(k)$ in Eq. S4, where $\boldsymbol{d}_i(k)$ is the Bloch vector of initial coin state for momentum k) and other topological systems.

Since the different robustness of the asymptotic entanglement of the quantum walk in different phases, it can be used to determine the phase boundary of the topological phases. As demonstrated in Fig. 3, although the exact value of the asymptotic entanglement changes for different initial states, it is always independently of the control parameter θ_2 in the non-trivial topological phase, and the phase boundaries can be further revealed.

2. ROBUSTNESS OF ENTANGLEMENT IN OTHER MODELS.

Actually, our previous argument about the robust asymptotic entanglement in the topological phase with $\mathcal{W} = 1$ is not only limited to the quantum walks system, it can feasible for more topological systems.

A. SSH model.

The Su-Schrieffer-Heeger (SSH) model [6], a one-dimensional topological insulator with the chirality symmetry, describes electrons hopping on a chain, which consists of N unit cells. In this model, each unit cell consists of two sites, one on sublattice A and one on sublattice B, and the hopping term connects the two sublattice sites. Hopping amplitudes v and ω represent the intracell hopping and intercell hopping, respectively. The dynamics of each electron is described by a single-particle Hamiltonian

$$\hat{H} = v\sum_{m=1}^{N}(|m,B\rangle\langle m,A| + h.c.) + \omega\sum_{m=1}^{N-1}(|m+1,A\rangle\langle m,B| + h.c.). \tag{S13}$$

Here, $|m,A\rangle$ and $|m,B\rangle$ are the states of the chain where the electron is in the cell m on sublattice A and B, respectively, and $h.c.$ represents the Hermitian Conjugate. The matrix $H(k)$ of the bulk momentum-space Hamiltonian can be expressed as

$$\begin{aligned} H(k) &= \begin{pmatrix} 0 & v+\omega e^{-ik} \\ v+\omega e^{ik} & 0 \end{pmatrix}, \\ H(k)\begin{pmatrix} a(k) \\ b(k) \end{pmatrix} &= E(k)\begin{pmatrix} a(k) \\ b(k) \end{pmatrix}. \end{aligned} \tag{S14}$$

The Bloch Hamiltonian is a 2×2 matrix

$$H(k) = E(k)n(k)\cdot\hat{\boldsymbol{\sigma}}. \tag{S15}$$

where $\hat{\boldsymbol{\sigma}}$ is the Pauli vector, $E(k)$ characterizes the typical band structure and $n(k)$ defines the direction of the eigenstates for each momentum k. The dispersion relation for the SSH model and components of the 3-dimensional vector $n(k)$ are given by

$$E(k) = |v+\omega e^{-ik}| = \sqrt{v^2+\omega^2+2v\omega\cos k}. \tag{S16}$$

$$\begin{aligned} n_x(k) &= \frac{v+\omega\cos(k)}{E(k)}, \\ n_y(k) &= \frac{\omega\sin(k)}{E(k)}, \\ n_z(k) &= 0. \end{aligned} \tag{S17}$$

The topological invariants can be characterized by the winding number $\mathcal{W}$, which counts the number of times the loop winds around the origin of the n_x, n_y plane. For the SSH model, the winding number $\mathcal{W}$ is 0 when $v > \omega$ and 1 when $v < \omega$. The band gap closes when $v = \omega$. In Fig. 4, we plot the phase diagram of the SSH model together with numerical simulations of the asymptotic entanglement between the internal (sublattice index A,B) and external degrees of freedom (unit cell index m) associated with an electron initially localized at a lattice site with initial parameters $\{\theta, \phi\} = \{\pi/2, 0\}$ after a long time evolution.

B. BCS theory of superconductivity.

We consider a one-dimensional superconductor with p-wave symmetry, and the effective Hamiltonian in momentum space is [7]:

$$H = \sum_k \Psi_k^\dagger H(k)\Psi_k \tag{S18}$$

with,

$$\Psi_k = \begin{pmatrix} c_k \\ c_{-k}^\dagger \end{pmatrix}, H(k) = \frac{1}{2}\begin{pmatrix} \epsilon(k) & \triangle k \\ \triangle k & -\epsilon(k) \end{pmatrix} \tag{S19}$$

where $\epsilon(k) = \frac{k^2}{2m} - \mu$ with $\frac{k^2}{2m}$ is the single-particle kinetic energy and μ is the chemical potential, $\triangle$ is the energy gap, $c_{k(-k)}$ and $c_{k(-k)}^\dagger$ are the annihilation and creation operators. Then we replace k and k^2 with $\sin k$ and $4[\sin(k/2)]^2$, respectively, to obtain the lattice effective model. The Bloch Hamiltonian

$H(k)$, dispersion relation $E(k)$, and the components of the 3-dimensional vector $n(k)$ are given by:

$$H(k) = E(k)n(k) \cdot \hat{\sigma}. \tag{S20}$$

$$E(k) = |\sqrt{(\triangle_k)^2 + (\epsilon_k)^2}|. \tag{S21}$$

$$\begin{aligned} n_x(k) &= \frac{\triangle_k}{E(k)}, \\ n_y(k) &= 0, \\ n_z(k) &= \frac{\epsilon_k}{E(k)}. \end{aligned} \tag{S22}$$

where $\triangle_k = \triangle \sin k$ and $\epsilon_k = \frac{[\sin(k/2)]^2}{m} - \mu$. The weak pairing phase ($\mu > 0$) is the non-trivial topological phase with $\mathcal{W} = 1$ and the strong pairing phase ($\mu < 0$) is the trivial topological phase with $\mathcal{W} = 0$. It is gapless only when $\mu = 0$ which separates two physical states. In Fig. 5, we plot numerical simulations of the entanglement between the internal and external degrees of freedom associated with an electron initially localized at a lattice site with initial parameters $\{\theta, \phi\} = \{\pi, \pi/2\}$ after a long time evolution.

REFERENCES

1. C. Yang, L. Li, and S. Chen, "Dynamical topological invariant after a quantum quench," Phys. Rev. B **97**, 060304 (2018).
2. T. Kitagawa, M. S. Rudner, E. Berg, and E. Demler, "Exploring topological phases with quantum walks," Phys. Rev. A **82**, 033429 (2010).
3. T. Kitagawa, "Topological phenomena in quantum walks: elementary introduction to the physics of topological phases," Quantum Inf. Process. **11**, 1107–1148 (2012).
4. O. Gamel and D. F. V. James, "Measures of quantum state purity and classical degree of polarization," Phys. Rev. A **86**, 033830 (2012).
5. F. Cardano, M. Maffei, F. Massa, B. Piccirillo, C. de Lisio, G. De Filippis, V. Cataudella, E. Santamato, and L. Marrucci, "Statistical moments of quantum-walk dynamics reveal topological quantum transitions," Nat. Commun. **7**, 11439 (2016).
6. W. P. Su, J. R. Schrieffer, and A. J. Heeger, "Solitons in polyacetylene," Phys. Rev. Lett. **42**, 1698 (1979).
7. N. Read and D. Green, "Paired states of fermions in two dimensions with breaking of parity and time-reversal symmetries and the fractional quantum hall effect," Phys. Rev. B **61**, 10267 (2000).

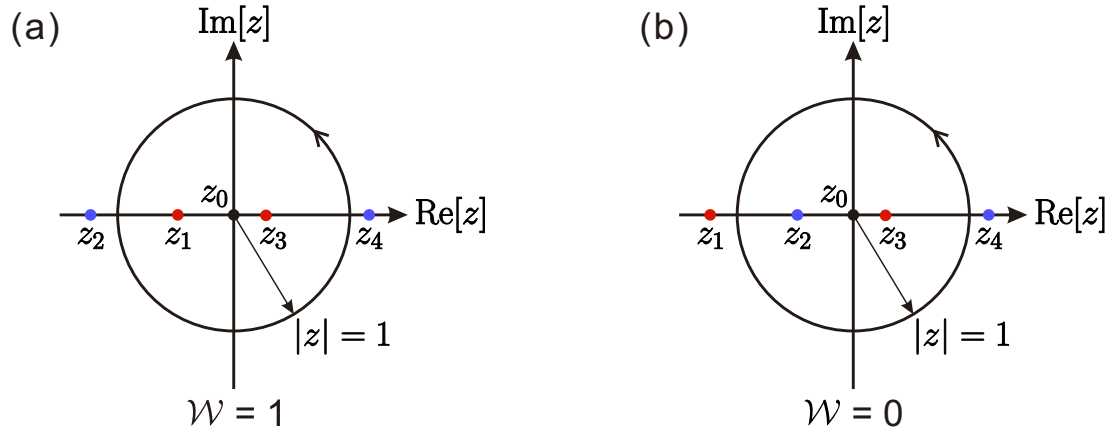

Fig. 1. The diagrammatic distribution of the poles (colored points) of $f(z)$ in the complex z-plane for (a) a non-trivial topological phase ($\mathcal{W} = 1$) with $\{\theta_1, \theta_2\} = \{\pi/2, \pi/5\}$ and (b) a trivial topological phase ($\mathcal{W} = 0$) with $\{\theta_1, \theta_2\} = \{\pi/2, 4\pi/5\}$. Apart from z_0, the paired poles $\{z_1,z_3\}$ or $\{z_2,z_4\}$ appearing in the unit circle $|z| = 1$ can cancel out the effect of parameter θ_2 on PP. When varying the θ_2, the locations of the poles z_1 or z_2 move along the real axis, exiting or entering the unit circle. Note that only the poles inside the unit circle have a contribution to the PP. For $\mathcal{W} = 1$, the valid poles are z_1 and z_3, which are a pair and can cancel out the effect of θ_2. While for $\mathcal{W} = 0$, the valid poles are z_2 and z_3, which are not a pair and can not cancel out the effect of θ_2.

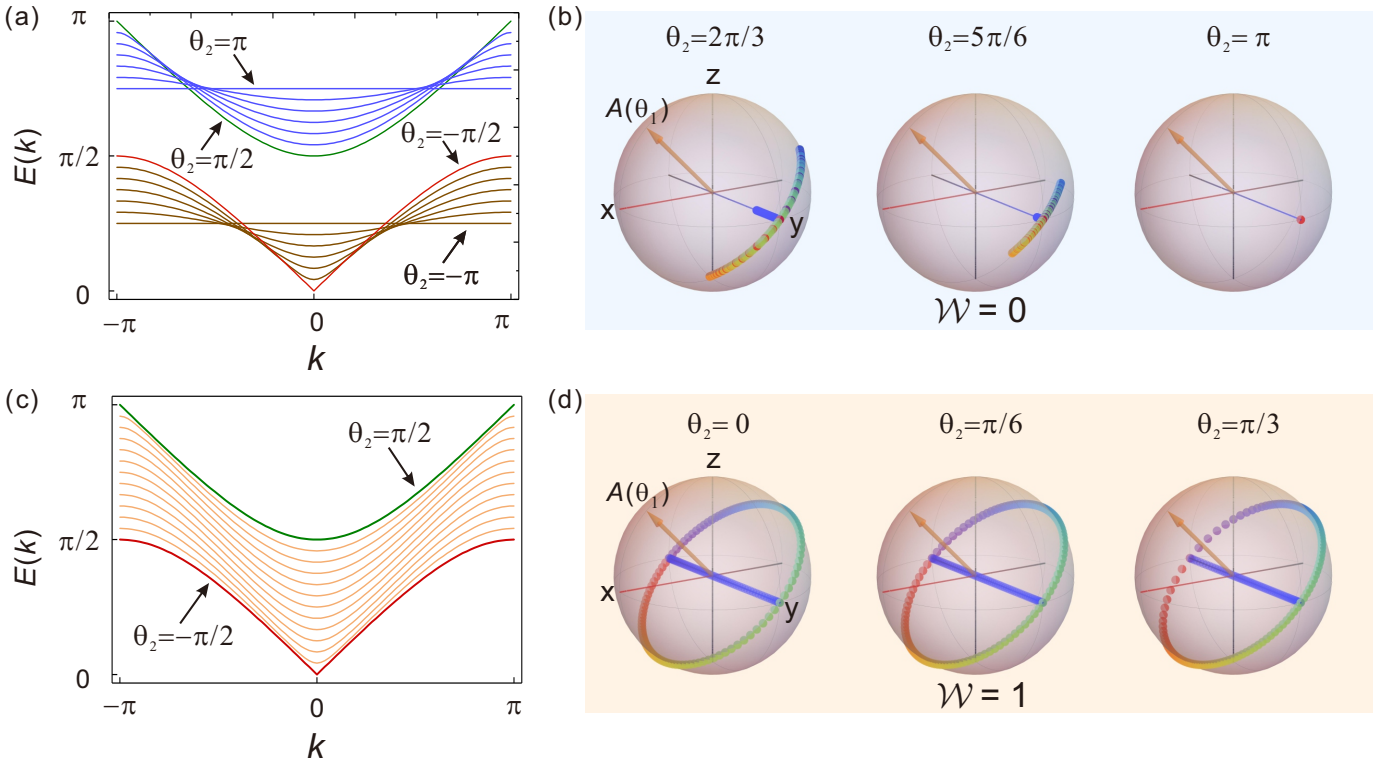

Fig. 2. The dispersion relation of quasi-energy $E(k)$ (left panel) and the winding of eigenvector $\boldsymbol{n}(k)$ accompanying with its y-component $n_y(k)$ (right panel) for the quasi-momentum $k \in [-\pi, \pi)$. We consider different θ_2 in (a-b) for trivial and (c-d) for non-trivial topological phases, respectively. The red and green lines in left panel stand for the topological phase transitions where a gap is closed at quasi-energy $E(0) = 0$ for $\theta_2 = -\pi/2$, and at $E(\pi) = \pi$ for $\theta_2 = \pi/2$, respectively. In (b), the winding of $\boldsymbol{n}(k)$ (colored points) forms an arc on the surface of Bloch sphere with its y-component $n_y(k)$ occupies a limit range (blue points), correspondingly, the energy range covered by the band $|E(\pi) - E(0)|$ increases (or decreases) with θ_2 (a). On the contrary, in the non-trivial topological phase, the energy band just shifts as the change of θ_2 and covers a stale range of energy ($|E(\pi) - E(0)| = \pi/2$ in this case) as shown in (c), correspondingly, $\boldsymbol{n}(k)$ winds around the vector $\boldsymbol{A}(\theta_1)$ always forming a closed circle, and its y-component $n_y(k)$ fully occupies y-axis all the time (d). Here we fix $\theta_1 = \pi/2$ and only show the upper band.

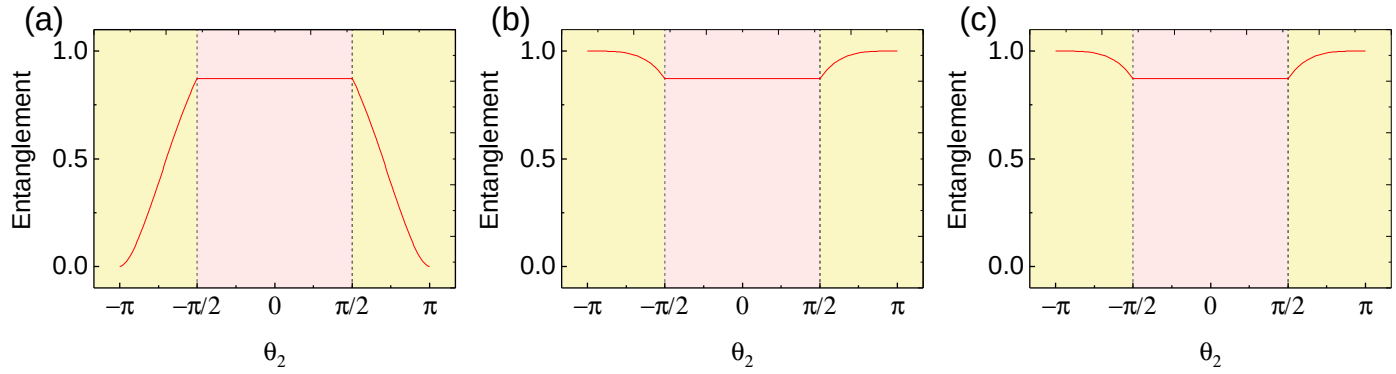

Fig. 3. Asymptotic entanglement as a function of parameter θ_2 for the initial state of the system (a) $\frac{1}{\sqrt{2}}(|H\rangle + i|V\rangle) \otimes |x = 0\rangle$, (b) $\frac{1}{\sqrt{2}}(|H\rangle + |V\rangle) \otimes |x = 0\rangle$ and (c) $|H\rangle \otimes |x = 0\rangle$ when θ_1 is $\pi/2$. The vertical black-dashed lines at $\theta_2 = \pm\pi/2$ show the phase boundaries. The asymptotic entanglement remains a constant in the region $\{-\pi/2, \pi/2\}$ (non-trivial topological phase) and increases or decreases in the two regions $\{-\pi, -\pi/2\}$ and $\{\pi/2, \pi\}$ (trivial topological phase). Independently of the specific initial state, we can obviously observe that the entanglement is independently of the control parameter θ_2 in the topological phase with $\mathcal{W} = 1$.

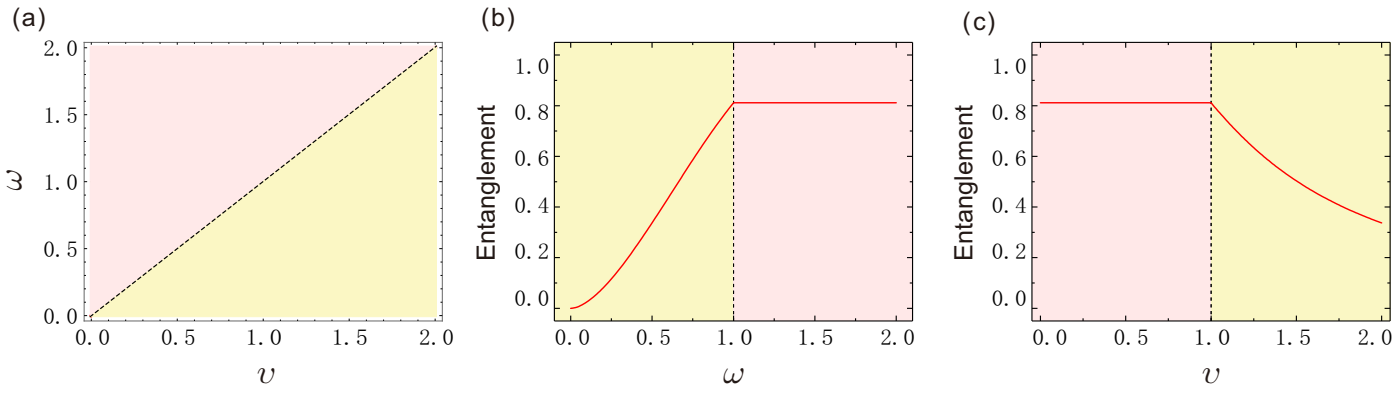

Fig. 4. (a) The phase diagram of the SSH model. The trivial topological phase in the yellow regions corresponds to winding number $\mathcal{W}$ that equals to 0 and the non-trivial topological phase in the pink regions corresponds to winding number $\mathcal{W}$ that equals to 1. The black-dashed line represents the phase boundaries between trivial and non-trivial topological phase. (b) and (c) show the numerical simulations of the asymptotic entanglement (red line) between internal and external degrees of freedom for the SSH model as a function of ω and υ, respectively. We vary the hopping amplitudes ω (υ) within the interval $\{0, 2\}$ when the hopping amplitudes υ (ω) is fixed as 1. It is clear that the entanglement is a constant in the non-trivial topological phase, and it dependents on ω and υ in the trivial topological phase. With the different robustness of entanglement, the phase boundary can be further obtained.

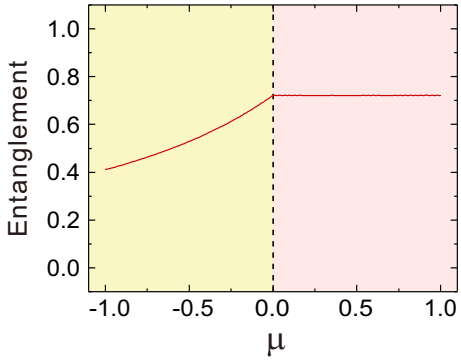

Fig. 5. Numerical simulations of the entanglement (red line) between internal and external degrees of freedom for the BCS model as a function of the chemical potential μ after a large number of steps. We vary the chemical potential μ within the interval $\{-1, 1\}$ when the energy gap $\triangle$ and $\frac{1}{m}$ are fixed as 1 and 3, respectively. The entanglement in the non-trivial topological phase (pink region) is a constant, i.e., more robust than the chemical potential μ in the trivial topological phase (yellow region). With the different robustness of entanglement, the phase boundary at $\mu = 0$ can be further obtained.

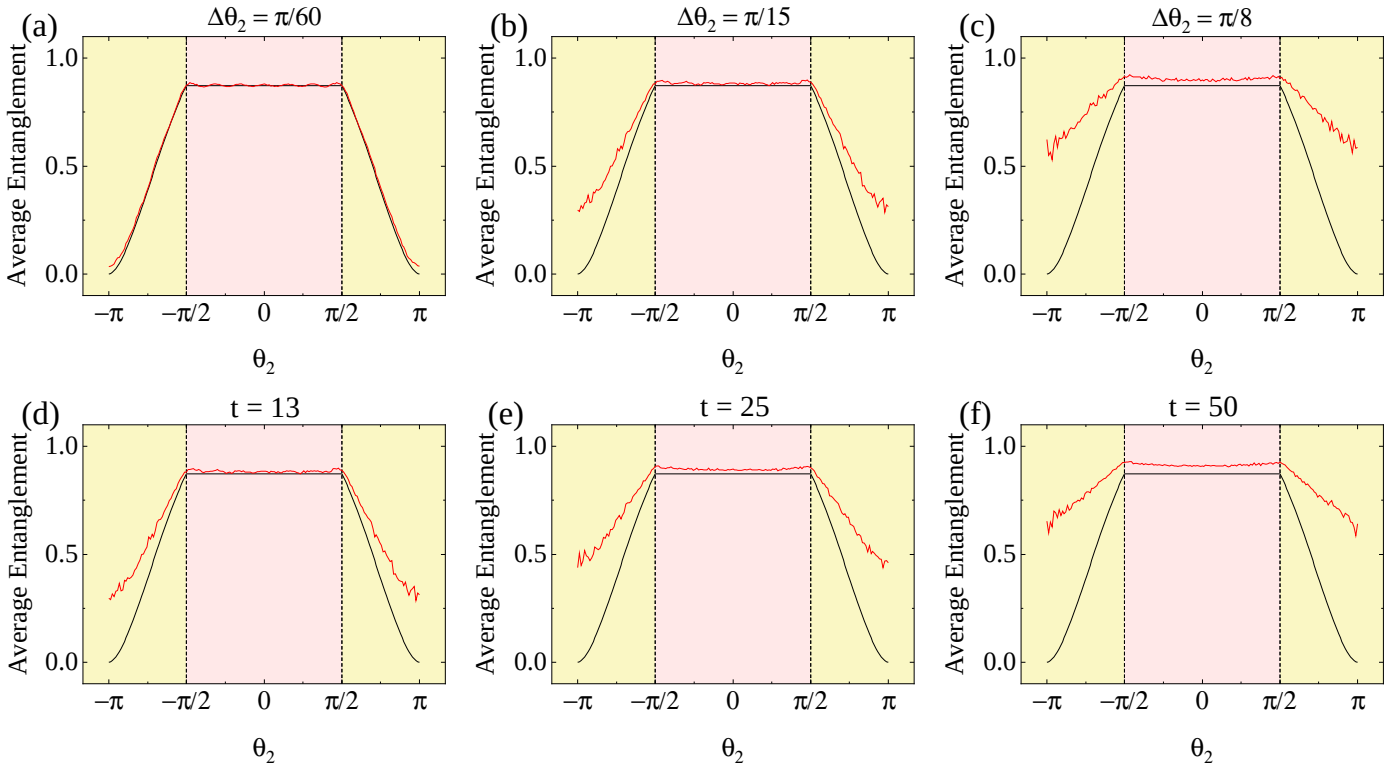

Fig. 6. Numerical simulations of the average entanglement in the presence of dynamic disorder in the split-step quantum walks staring from a localized state $|x = 0\rangle \otimes |\downarrow_y\rangle$. In this simulation, the first parameter θ_1 is fixed as $\pi/2$, and dynamic disorder is introduced via random fluctuations of the second parameter θ_2 at each step. In (a-c), we numerically calculate the average values of the entanglement (red lines) with three different random disorder strengths $\Delta\theta_2 = \pi/60$, $\pi/15$ and $\pi/8$ while varying θ_2 in the range $\{-\pi, \pi\}$ for a walk of 13 steps. The black-solid lines represent the asymptotic entanglement without random disorder. As shown in (a-b), it can be observed that the average entanglement in the topologically non-trivial phase is almost invariant when the strength of disorder is small (chirl-preserving disorder). With increasing disorder strength, the disorder will destroy the topological character of system and the associated invariant of average entanglement (shown in (c)). In (d-f), the average entanglement calculated for a 13-, 25- and 50-step walk in the presence of disorder with strength $\Delta\theta_2 = \pi/15$ is shown. We can see that the average entanglement in the topologically non-trivial phase is almost invariant when the number of the steps is small. As the increase of evolution time, the invariant of average entanglement in the topologically non-trivial phase will be destroyed. The number of samples is 100 in (a-f).